

Pulse-width and isotope effects in femtosecond-pulse strong-field dissociation of H_2^+ and D_2^+

C. Trump,¹ H. Rottke,¹ M. Wittmann,¹ G. Korn,¹ W. Sandner,^{1,2} M. Lein,^{3,4} and V. Engel³

¹Max-Born-Institut, Max-Born-Straße 2a, D-12489 Berlin, Germany

²Technische Universität Berlin, Hardenbergstraße 36, D-10623 Berlin, Germany

³Institut für Physikalische Chemie, Am Hubland, D-97074 Würzburg, Germany

⁴Institut für Theoretische Physik, Am Hubland, D-97074 Würzburg, Germany

(Received 29 March 2000; published 30 October 2000)

Using a high-resolution setup, we investigate the fragmentation of H_2 and D_2 in intense 790 nm laser pulses with pulse widths of 28 fs and 80 fs. The measured H^+ (D^+) kinetic energies resulting from effective two-photon dissociation of H_2^+ (D_2^+) show a clear dependence on the pulse width and on the isotope. One-dimensional calculations reproduce these effects and show that they mainly originate from the H_2^+ (D_2^+) dissociation dynamics. Further, we find that the initial ionic state before dissociation is not simply given as a Franck-Condon distribution over unperturbed ionic states. Rather it is a complex mixture of initial wave packets (covering, however, a small energy range) created by multiphoton ionization of H_2 and D_2 at various times during the action of the pulse.

PACS number(s): 33.80.Rv, 42.50.Hz

I. INTRODUCTION

Since the first experimental discovery of bond softening and effective two-photon dissociation of H_2^+ in intense ultrashort laser pulses [1,2], several recent publications have tried to investigate and interpret the detailed shape of the proton kinetic-energy distribution emerging from these dissociation processes [3–6]. Unperturbed ionic vibrational levels where dissociation starts have been deduced from the proton kinetic-energy distribution [1–5]. Gibson *et al.* and Walsh *et al.* [3,4] tried to interpret the shape of the bond-softening and effective two-photon dissociation lines by assuming that they are determined by an initial Franck-Condon (FC) distribution over unperturbed ionic vibrational states formed in the multiphoton ionization (MPI) of the H_2 molecule. The FC distribution seemed to fit experimental results quite well [4]. This interpretation of the line shape ignores completely possible dynamical effects which may also influence the final proton kinetic-energy distribution. Also it does not take into account that, at the light intensity where effective MPI of H_2 starts, the vibrational structure of the ion is already strongly perturbed by the electric field of the light pulse. It was shown by Sukharev and Krainov [7] that Franck-Condon factors for H_2 ionization become dependent on the external perturbation at experimentally relevant light intensities. Numerical simulations and comparison with experiment revealed that the intensity dependence found for the two ionic dissociation channels is a critical function of the initial conditions assumed [6].

In order to reveal details of the ionic dissociation dynamics we measure the kinetic-energy distribution of dissociation products with high resolution and investigate its dependence on the light pulse width. With the pulse width reaching the time scale for dissociation of the molecular hydrogen ion it is found that the shape and position of the effective two-photon dissociation line becomes dependent on the isotopic species (H_2 or D_2) used in the experiment. This indicates that the detailed dissociation dynamics and not only the initially prepared ionic “state” (by MPI of the neutral molecule) influ-

ences the final kinetic-energy distribution of the dissociation products.

We compare the experimental results with one-dimensional simulations of the fragmentation in ultrashort intense light pulses. The calculations confirm that, under the given conditions, the time evolution during dissociation depends on the isotope and on the pulse duration, which qualitatively explains the experimentally observed results. For a full understanding, it turns out that the preparation of the initial ionic state must be studied in detail. In particular, we find that the major contribution to two-photon fragmentation is not necessarily from molecular ions created by MPI at mid-pulse, but rather from ions created on the leading or falling edge of the pulse.

II. EXPERIMENTAL SETUP

A supersonic beam setup combined with an electric-field-free ion time-of-flight spectrometer was used to investigate the kinetic-energy distribution of ions formed by photodissociation. It has an overall kinetic-energy resolution for H^+ ions of $\Delta E/E=0.05$ in the range $E \leq 10$ eV, mainly determined by the geometry of the spectrometer. The main improvement in energy resolution can be attributed to the supersonic molecular beam. Compared to the conventional method of using a thermal gas ($kT=25$ meV) as target instead of the supersonic beam, the resolution, e.g., for H^+ ions is improved at least by a factor of 10 (limitations due to the spectrometer setup in the case of a thermal gas are not taken into account) [8,9]. The molecular-beam setup eliminates the thermal velocity spread present in a bulk gas sample which mainly limited the resolution in previous experiments.

Two different Ti:sapphire laser systems delivering ultrashort light pulses were used to excite the molecules. Both of them are based on a Kerr lens mode-locked oscillator followed by chirped-pulse amplification stages. The center wavelength of the light pulses was at ≈ 790 nm. Laser system I delivered pulses amplified to pulse energies of up to 600 μJ at 1 kHz repetition rate. The pulse width in this case

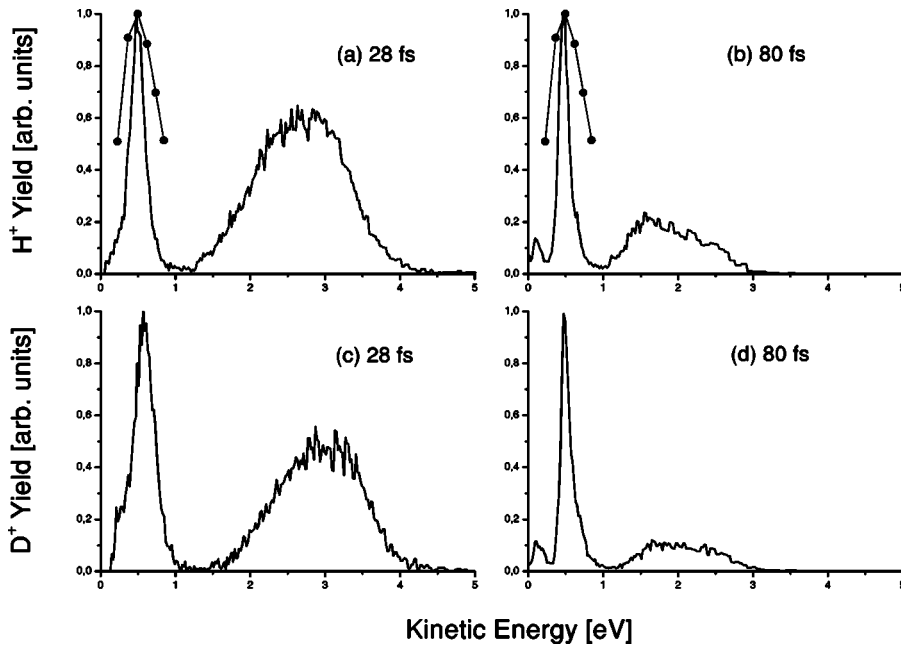


FIG. 1. The H^+/D^+ ion kinetic-energy distribution at two different light pulse widths τ_p . (a) H^+ at $\tau_p=28$ fs, (b) H^+ at $\tau_p=80$ fs, (c) D^+ at $\tau_p=28$ fs, (d) D^+ at $\tau_p=80$ fs. The peak laser intensity was kept fixed at 5×10^{14} W/cm^2 .

was 28 fs full width at half maximum (FWHM) of a Gaussian pulse. The laser light beam was focused by a spherical mirror with a focal length of 250 mm to excite the hydrogen molecules. In this way, effects of material dispersion on the pulse characteristics in the focal spot were eliminated. The output of laser system II consisted of pulses with a duration of 80 fs (FWHM of a Lorentzian pulse) at a lower repetition rate of 10 Hz. The pulse energy reached up to 4 mJ. A fused silica lens with a focal length of 260 mm was used to focus this laser beam on the molecular-beam target.

The experimental setup consisted of a supersonic jet source, a differentially pumped transport and collimation stage for the beam, and an ultrahigh-vacuum (UHV) chamber where the molecules were excited by the laser light. Details of the experimental setup can be found in [8]. The mean velocity of hydrogen and deuterium in the beam was 2470 ± 150 and 1750 ± 100 m/s, respectively. The free jet expansion cooled the translational degrees of freedom of the molecules. Estimated from measurements [8], a speed ratio higher than ≈ 20 was reached. This corresponds to a velocity spread of ± 65 m/s (± 45 m/s) for H_2 (D_2) along the molecular-beam axis. The transverse spread is geometrically fixed by apertures placed in the collimation stage and is less than $\approx \pm 5$ m/sec.

With the 10-Hz-repetition-rate laser system we used a pulsed nozzle with an orifice 0.1 mm in diameter to form the molecular beam. At a backing pressure of ≈ 3 bar, the gas pulse width of this source was ≈ 150 μs . With the 1 kHz laser we switched to a cw nozzle to limit the gas flow at the backing pressures necessary for reasonable cooling of the molecules. The orifice of this nozzle was 10 μm in diameter. To maintain approximately equal particle densities in the interaction region we adapted the length of the molecular-beam transport stage to the different gas flows through the nozzles.

The base pressure in the UHV vacuum chamber where the focused laser beam excited the molecules was below 1

$\times 10^{-9}$ mbar. In the focal spot, the particle density in the molecular beam was always kept low enough to eliminate space-charge effects on the kinetic-energy distribution of the ions.

We used an electric-field-free technique to measure the angle-resolved kinetic-energy distribution of H^+ and D^+ fragment photoions emitted along the molecular-beam axis. The acceptance angle of the flight tube was $\pm 2.3^\circ$ with respect to the spectrometer axis [8]. At small kinetic energy the acceptance angle becomes energy dependent; it rises with decreasing kinetic energy of the fragments [8]. The time of flight of single ions was measured by a time to digital converter, which was capable of multiple stops and had a time resolution of 1 ns. In all experiments, the direction of linear polarization of the laser beam was set parallel to the spectrometer axis.

III. EXPERIMENTAL RESULTS AND DISCUSSION

Figure 1 shows H^+ and D^+ ion kinetic-energy distributions formed by ionization/dissociation of H_2 and D_2 , respectively, at two different laser pulse widths τ_p . The peak intensity of the light pulses in the interaction volume of the light beam with the molecules was kept fixed at 5×10^{14} W/cm^2 for all spectra. The overall shapes of the spectra are similar. The processes giving rise to the various peaks in the spectra have been discussed in various previous publications [1–6,10,11]. They are only briefly recapitulated here.

In the high-intensity light pulse H_2 (D_2) initially becomes photoionized near the equilibrium internuclear separation through a vertical Franck-Condon type of transition. Following ionization, the molecular ion starts dissociating [1–6,10,11]. The dissociation can be visualized as taking place on dressed potential curves in the Floquet picture [12]. In the Floquet one-photon channel, a single photon is effectively absorbed during dissociation (bond-softening dissociation [1]). It gives rise to products with a kinetic energy near

TABLE I. Position and width (FWHM) of the effective two-photon dissociation line in Fig. 1.

Isotope	τ_p	Position	FWHM
H ⁺	28 fs	0.47 eV	230 meV
D ⁺	28 fs	0.57 eV	310 meV
H ⁺	80 fs	0.47 eV	160 meV
D ⁺	80 fs	0.47 eV	140 meV

170 meV. As can be seen in Fig. 1, a distinct line structure corresponding to dissociation in the one-photon channel is observed only when the molecules are excited with the 80 fs light pulses. The disappearance of the line structure for short laser pulses was also observed by Frasinski *et al.* [13]. In the Floquet two-photon channel, the molecular ion first absorbs three photons at small internuclear separation and starts dissociation. At an increased internuclear separation it is stimulated by the light to emit one photon [10,4,3,5,6], thereby undergoing an effective two-photon dissociation. Via this channel, products with kinetic energy of about 0.5 eV are formed (see Fig. 1). The dissociating H₂⁺ (D₂⁺) ions pass through a range of internuclear separations where charge resonant enhanced ionization (CREI) may happen in the strong electric field of the light wave [14–17]. This gives rise to a locally enhanced photoionization rate and initiates Coulomb explosion of the then bare nuclei. This process is responsible for the broad structures observed in the spectra between 1 eV and 4 eV.

The attention of this article mainly focuses on effective two-photon dissociation. In all experiments up to now, no marked dependence of the kinetic-energy release on the light pulse duration and on the isotopic species in the two-photon channel was observed to our knowledge. The independence of the isotope seemed to indicate that dissociation is mainly determined by the electronic properties of the neutral molecule and the ion. However, the experimental spectra we

took at light pulse widths of 80 fs and 28 fs reveal evident pulse-width and isotope effects (see Fig. 1). In Table I we have summarized the position and width of the two-photon dissociation line. Three main features can be observed: (1) An isotopic shift of the peak position (from 0.47 eV to 0.57 eV) for the short laser pulses. The isotopic shift is not visible in the experiment with 80 fs laser pulses. The position of the three lines in Figs. 1(a), 1(b), and 1(d) remains fixed. (2) An increase of the line width with decreasing pulse width. (3) The appearance of a shoulder on the low-energy side of the line in the experiment with the shorter laser pulses ($\tau_p = 28$ fs). The shoulder is more pronounced for the D⁺ kinetic-energy distribution (see also Fig. 2). For the 80 fs pulses the two-photon dissociation line shows a sharp cutoff on the low-energy side, which is most pronounced for D₂.

To exclude the possibility that the light intensity has any effect on the two-photon line, we measured the intensity dependence of the H⁺ (D⁺) kinetic-energy distribution in the range from 5×10^{14} W/cm² to 2×10^{15} W/cm² for both setups. A representative intensity dependence of the D⁺ kinetic-energy distribution for 28 fs pulses is shown in Fig. 2. The result for all the spectra is the same. The position and width of the effective two-photon dissociation line do not change on varying the light intensity. In contrast, the Coulomb explosion peak is shifted toward higher energies with increasing intensity. Also, the ratio of the area under the Coulomb explosion peak to that under the effective two-photon dissociation peak increases. This high-intensity behavior of the effective two-photon dissociation line was already pointed out by Thompson *et al.* [5] and by Posthumus *et al.* [18]. These authors concluded that dissociation in this channel is observed only from regions of the focused light beam where the intensity is between 1×10^{14} and 3×10^{14} W/cm².

In the proton kinetic-energy distributions in Figs. 1(a) and 1(b) we have shown how the effective two-photon dissociation line would look if an initial Franck-Condon distribution

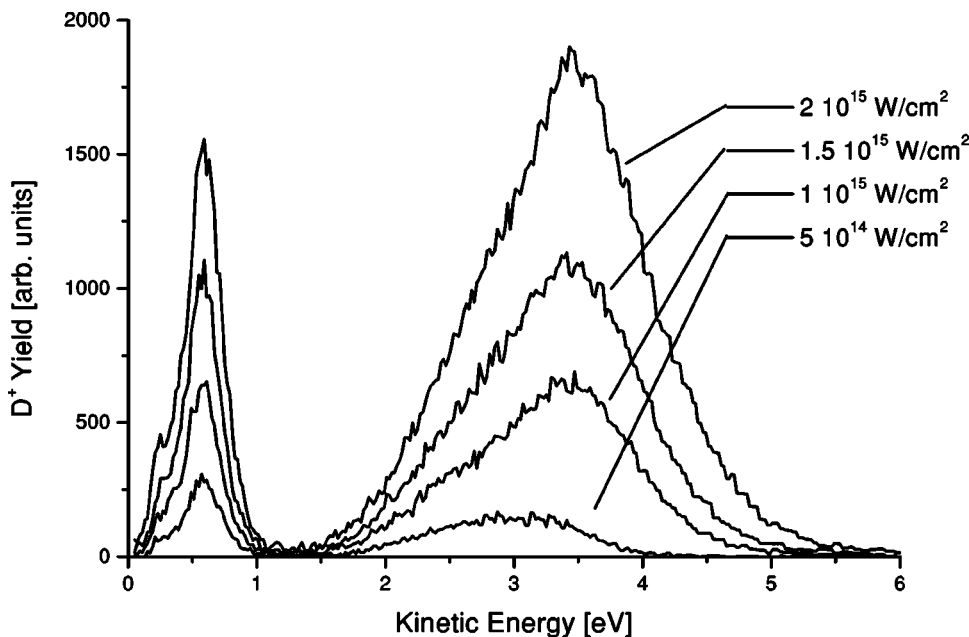


FIG. 2. D⁺ ion kinetic-energy distributions measured at different light intensities, as indicated. The light pulse width was 28 fs.

over unperturbed H_2^+ vibrational levels in the electronic ground state, created in the H_2 MPI step, alone determined the shape of the line. The connected dots represent the line shape expected in this case. The Franck-Condon factors for the different vibrational states (starting with $v=0$ at the lowest kinetic energy) are given relative to the FC factor for $v=2$, which was arbitrarily set to 1. It is immediately obvious that the observed line is much narrower than the ‘‘FC line.’’ In terms of unperturbed ionic vibrational states, the maximum of the observed effective two-photon dissociation line appears at a kinetic energy where one expects to find protons from two-photon dissociation of the ionic vibrational state $v=2$ [see Figs. 1(a) and 1(b)]. At 80 fs light pulse width, the neighboring vibrational states seem to contribute only little to effective two-photon dissociation. Their contribution seems to increase with decreasing light pulse width. In the case of D_2 , the maximum of the observed effective two-photon dissociation line appears at an energy where one would expect deuterons from dissociation of the unperturbed $v=3$ vibrational state. There may be two reasons for the deviation of the experimental results from a FC distribution. Either MPI of the neutral molecules at high light intensity cannot be visualized as a vertical FC transition between unperturbed electronic states, or dynamical effects during dissociation determine the final kinetic-energy distribution of the dissociation products. The simulations below will shed light on this point.

Concerning the experimentally determined kinetic-energy distributions, the question remains: what influences the width of the effective two-photon dissociation line? The energy resolution of the experimental setup is 25 meV at 500 meV kinetic energy where the two-photon dissociation line appears. It therefore contributes only little to the observed line-width. Especially in the case of hydrogen a second non-negligible contribution to the line width may originate in the initial MPI step of the neutral molecule. The H_2^+ ion experiences a recoil momentum from the leaving photoelectron. Since at the light intensities used in the experiment the momentum of the mechanical system (H_2, D_2) is conserved nearly exactly in the photoionization step, the momentum of the photoion is equal to the electron momentum but directed in the opposite direction [19]. We detected dissociation products along the axis of polarization of the light beam. Along this direction, photoelectrons are found with kinetic energies of up to about 5 eV. The photoelectrons and therefore also the H_2^+ and D_2^+ ions thus have momenta in the range between -0.6 a.u. and $+0.6$ a.u. along this direction. This momentum distribution contributes to the width of the two-photon dissociation line since dissociation starts from a moving molecular ion. Based on the photoelectron momentum distribution, one estimates for the H^+ (D^+) linewidth that a portion of up to 140 meV (100 meV) originates from the recoil momentum of the molecular ion. This estimation indicates that at 80 fs pulse width the major part of the observed linewidth stems from recoil (see Table I). At the short pulse duration, the dissociation mechanism contributes significantly to the observed linewidth. The fact that the peak is considerably broadened by recoil in all cases supports the statement made above that only a small band of states of the

molecular ions is involved in effective two-photon dissociation.

IV. THEORETICAL MODEL

It is currently not feasible to simulate the complete process of multiphoton fragmentation of H_2 and D_2 . Hence we adopt two approximations that have frequently been used in numerical calculations. The first is that the initial ionization is considered a sudden process leading from the ground state of the molecule to the electronic ground state of the molecular ion. The internuclear separation is assumed to remain unchanged during ionization. In this way we fix the initial state for the subsequent dynamics of the molecular ion. The second approximation is that the entire process is treated in a linear model, i.e., nuclear and electronic motion are restricted to the axis of the laser polarization. A one-dimensional (1D) description of the nuclei is reasonable because the dissociating molecular ions are forced to be aligned with the polarization axis [20]. As far as the electronic degree of freedom is concerned, previous studies have shown that strong-field phenomena are qualitatively reproduced in linear models [21,22].

A 1D model with fixed nuclei was used to study CREI of the H_2 molecule in intense laser fields [23]. For H_2^+ , a non-Born-Oppenheimer 1D model with one nuclear and one electronic degree of freedom was introduced by Kulander *et al.* [24]. Recently, it has been used to study the dissociation in strong 150 fs pulses [6]. These are the models that we employ in the present work. They involve smoothed potentials for the electron-electron and electron-nucleus interactions (soft Coulomb potentials).

The ionization of H_2 (D_2) can happen at any time t_0 during the interaction with the light pulse. There is no *a priori* reason to choose a particular t_0 . Therefore, we use a two-step computational procedure consisting of (i) ionization of the molecule and (ii) dissociation of the molecular ion.

First, we calculate the time-dependent single-ionization probability of H_2 (D_2). Here, the internuclear distance is held fixed at the equilibrium separation R_0 in the electronic ground state. In the linear model, the Hamiltonian reads [23] (atomic units are used)

$$H_{R_0} = \sum_{k=1,2} \left\{ -\frac{1}{2} \frac{\partial^2}{\partial z_k^2} - \frac{1}{\sqrt{(z_k - R_0/2)^2 + 1}} - \frac{1}{\sqrt{(z_k + R_0/2)^2 + 1}} \right\} + \frac{1}{\sqrt{(z_1 - z_2)^2 + 1}} + E_0 f(t) \sin(\omega t) (z_1 + z_2), \quad (1)$$

where z_1, z_2 are the electron coordinates relative to the center of the two nuclei, E_0 is the peak amplitude of the electric field, $f(t)$ is an envelope function, and ω is the laser frequency. The two-electron wave function is represented numerically on a two-dimensional grid with absorbing boundaries. The spatial step size is 0.32 a.u. and the size of the grid is 164×164 a.u. We use the split-operator method [27] with 1500 time steps per optical cycle to propagate the wave func-

tion. The time evolution starts from the ground state, which is obtained by propagation in imaginary time. We define the ionization probability as the probability for one electron to leave the grid, while the other remains within some region $|z| < z_b$. We find that the ionization probability depends only slightly on z_b if its value is chosen larger than about 5 a.u. This is plausible since more than 99% of the electronic ground state density is located within $|z| < 4$ a.u. In the calculations we use $z_b = 7$ a.u. The time-integrated ionization probability increases in a stepwise fashion with one step per half optical cycle. It is therefore reasonable to extract the ionization probability per half cycle.

After ionization at $t = t_0$, the dissociation dynamics of the 1D molecular ion is governed by the Hamiltonian [24]

$$H = -\frac{1}{2\mu_e} \frac{\partial^2}{\partial z^2} - \frac{1}{m_n} \frac{\partial^2}{\partial R^2} + \frac{1}{R} - \frac{1}{\sqrt{(z-R/2)^2 + 1}} - \frac{1}{\sqrt{(z+R/2)^2 + 1}} + \kappa z E_0 f(t) \sin(\omega t) \quad (2)$$

with

$$\mu_e = \frac{2m_n}{2m_n + 1}, \quad \kappa = \frac{2m_n + 2}{2m_n + 1}. \quad (3)$$

Here, R is the internuclear distance, z is the electron coordinate relative to the center of the nuclei, and m_n is the nuclear mass. As initial state of the molecular ion we use

$$\Psi(z, R, t = t_0) = \Phi_0^{H_2(D_2)}(R) \Psi_R(z), \quad (4)$$

where $\Phi_0^{H_2(D_2)}(R)$ is the vibrational ground state of one-dimensional H_2 (D_2) (obtained as the square root of the nuclear density that was taken from a 1D non-Born-Oppenheimer calculation) and $\Psi_R(z)$ is the electronic ground state of one-dimensional H_2^+ (D_2^+) at fixed nuclear separation R (electronic Born-Oppenheimer wave function). With Eq. (4) we assume that there is a sudden transition at $t = t_0$ from the total ground state of H_2 (D_2) into the *electronic* ground state of H_2^+ (D_2^+) without changing the nuclear wave function. We restrict ourselves to initial times t_0 when the electric field is zero to prevent unphysical switch-on effects. The size of the numerical grid is 77 a.u. for the nuclear coordinate and up to 164 a.u. for the electronic coordinate. The spatial step size is 0.075 a.u. for the nuclear degree of freedom and 0.32 a.u. for the electronic degree of freedom. The propagation in time is done with 1024 split-operator steps per optical cycle.

The envelope function $f(t)$ is taken to be a \sin^2 function. The width τ_p of an experimental laser pulse is defined as the FWHM of the time-dependent intensity curve. Under assumption of a Gaussian pulse, τ_p is related to the FWHM τ_E of the electric field amplitude by $\tau_E = \sqrt{2}\tau_p$. For any given τ_p , the duration of the \sin^2 pulse used in the calculation is taken such that the FWHM of its amplitude is also equal to $\sqrt{2}\tau_p$. The total pulse duration is then equal to $\sqrt{8}\tau_p$.

In the present study, we are primarily interested in the two-photon dissociation. It has been shown previously that

for peak intensities as large as 5×10^{14} W/cm² the fragmentation of H_2 into $H + H^+$ does not occur in the center of the laser focus, but only in the shell with intensities in the range $(1-3) \times 10^{14}$ W/cm² [5,18]. This is confirmed by our simulations, where the two-photon peak is mainly produced at intensities around 1.5×10^{14} W/cm², and by the insensitivity of the shape of the effective two-photon dissociation line to light intensity in the experimental spectra (Fig. 2). We therefore choose laser parameters of $E_0 = 0.0654$ a.u. and $\omega = 0.0577$ a.u., corresponding to $I = 1.5 \times 10^{14}$ W/cm² and $\lambda = 790$ nm.

The grid for H_2^+ (D_2^+) is chosen large enough in the nuclear coordinate to ensure that the nuclear wave packets do not reach the boundary within the propagation time. The final wave function then consists of a bound portion Ψ_b at $R \sim 2-4$ a.u. and a fragmented portion Ψ_f at large R . We obtain Ψ_f by smoothly cutting off the inner part $R < R_b = 5$ a.u. We note that the results are not sensitive to the precise choice of R_b . The nuclear-momentum distribution of Ψ_f is obtained by integrating the squared modulus of its momentum-space representation over the electronic degree of freedom. Then the kinetic-energy spectrum of the fragments follows by transformation of the momentum distribution to the energy scale [6]. The total kinetic-energy release is equally shared by the two fragments if we neglect ionization recoil effects and energy transfer to the center-of-mass motion of the molecular ion. Thus, the *ion* kinetic energies that we present in Sec. V are simply one-half of the total kinetic-energy release.

At the edge of the grid we use absorbing boundary conditions for the electron. Thus, information is lost about those parts of the wave function that undergo ionization. As a consequence, the channel $H^+ + H^+$ resulting from Coulomb explosion is not present in the kinetic-energy spectrum that we calculate from the final wave function. (For study of the Coulomb explosion, a wave-function splitting technique can be used to propagate the ionized parts of the wave function [6].)

V. NUMERICAL RESULTS

We have performed calculations for both H_2 and D_2 , and for three different pulse durations, $\tau_p = 30, 50,$ and 80 fs. Let us first discuss the ionization of H_2 (D_2), which does not depend on the isotope because we fix the nuclei at the equilibrium distance $R_0 = 2.2$ a.u. The single-ionization probability is shown in Fig. 3(b) for $\tau_p = 80$ fs, in Fig. 4(b) for $\tau_p = 50$ fs, and in Fig. 5(b) for $\tau_p = 30$ fs. At each time t when the electric field is zero, a vertical bar indicates the ionization probability during the half cycle immediately before t . The most striking feature in these plots is that, for $\tau_p = 80$ fs and $\tau_p = 50$ fs, ionization is most effective at times before mid-pulse (denoted as t_3). A second, smaller maximum in the ionization is found on the falling edge of the pulse. In the case of a 30 fs pulse, the time-dependent ionization exhibits a similar shape, except that the first maximum is located at the middle of the pulse. These effects seem to be related to stabilization phenomena that were found (although for higher laser frequencies) in previous

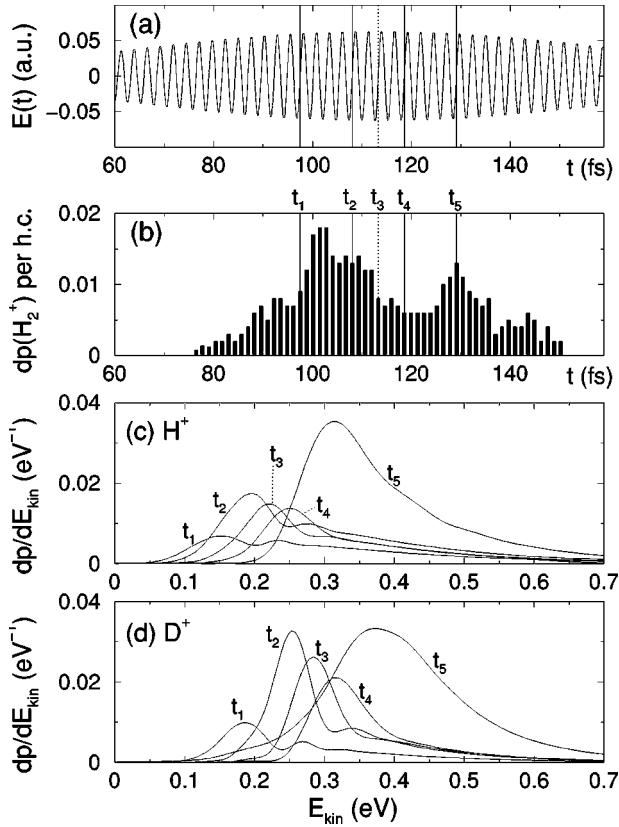


FIG. 3. Calculated fragmentation of H_2 (D_2) in an 80 fs pulse with a peak intensity of $1.5 \times 10^{14} \text{ W/cm}^2$. (a) Time-dependent laser field. (b) Single-ionization probability per half optical cycle. (c),(d) Kinetic-energy spectra of H^+ (D^+) for different ionization times, weighted by the corresponding ionization probabilities.

simulations (see [25] and references therein, and also [26]). The comparatively large ionization rates on the leading and falling edges of the pulse can be due to either nonadiabatic projection onto continuum states (caused by the intensity *change*), or “adiabatic stabilization” making the molecule more stable against ionization at larger intensities (independent of the pulse shape).

For various times of ionization (denoted as t_n , $n = 1, \dots, 5$, in Figs. 3–5), we have calculated the kinetic-energy spectra of the ions H^+ (D^+). Panels (c) and (d) of Figs. 3–5 show the results. To assess the contribution of a particular ionization time, we have weighted each kinetic-energy spectrum with the corresponding ionization probability of panels (b). Here and in the following, we assume that the probability for the start of dissociation at time t_n is given by the ionization probability during the half cycle immediately before t_n . Note that the energy scale in panels (c) and (d) is very much stretched as compared to Fig. 1. The figures demonstrate that the kinetic-energy release depends strongly on the time of ionization. In general, ionization at a later time leads to a *broader* peak located at *higher* energies. A comparison of the two isotopes at equal ionization times shows that D^+ usually acquires a larger energy than H^+ . For very late ionization times [see t_5 in Figs. 4(d) and 5(c), and t_3, \dots, t_5 in Fig. 5(d)], additional contributions at low energy appear. We believe that these low-energy fragments are

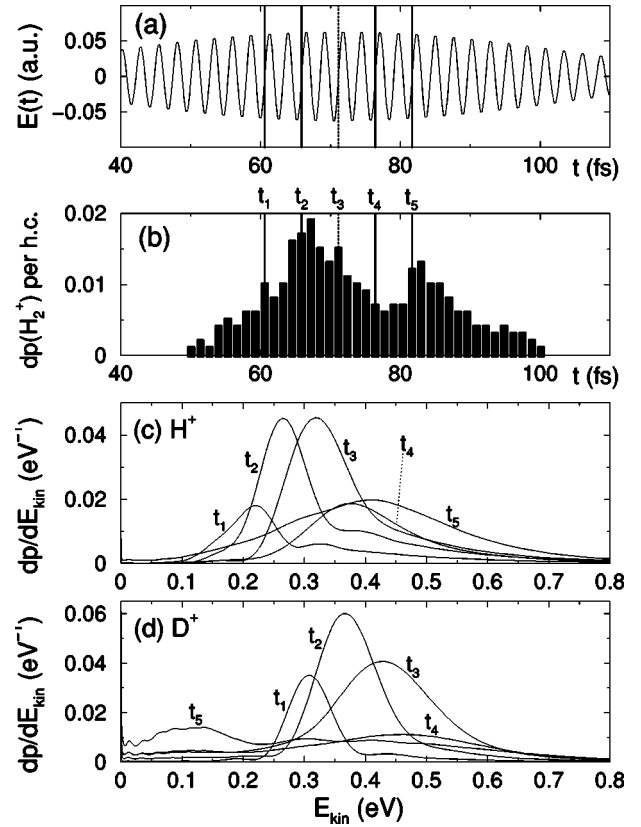


FIG. 4. Same as Fig. 3, but for a 50 fs pulse.

responsible for the shoulder that is experimentally observed on the low-energy side of the two-photon peak for short pulses. We find that in all cases shown in Fig. 3 (80 fs pulse) and Fig. 4 (50 fs pulse), the final wave function has gerade symmetry, which means that the fragmentation results from an effective two-photon absorption. For the 30 fs pulse width, on the other hand, the low-energy maxima belonging to t_5 in Fig. 5(c) and t_4, t_5 in Fig. 5(d) are mainly due to one-photon absorption. Apparently, the low-energy shoulder is in general formed by a mixture of one-photon and two-photon fragments.

At this point, we remind the reader that one-photon dissociation is certainly occurring as well for long pulse durations, but only at the lower intensities in the outer regions of the spatial intensity distribution in the laser focus. In our calculation, the intensity was chosen such that two-photon dissociation is the predominant process.

From Figs. 3–5 we conclude that a wide range of ionization times contributes, and it is not sufficient to restrict the analysis to a particular one. Instead, one should add up all contributions, properly weighted with the ionization probability at each time. If we had access to the wave function of the entire system, consisting of molecular ion plus ionized electron, we could add these contributions coherently. However, the information about the electron is lost. Thus, the relative phases of the contributions belonging to different ionization times are unknown. Therefore, we compute the incoherent sum. This is an approximation that would be exact if the state $|\phi_{t_i}\rangle$ of the ionized electron for ionization at

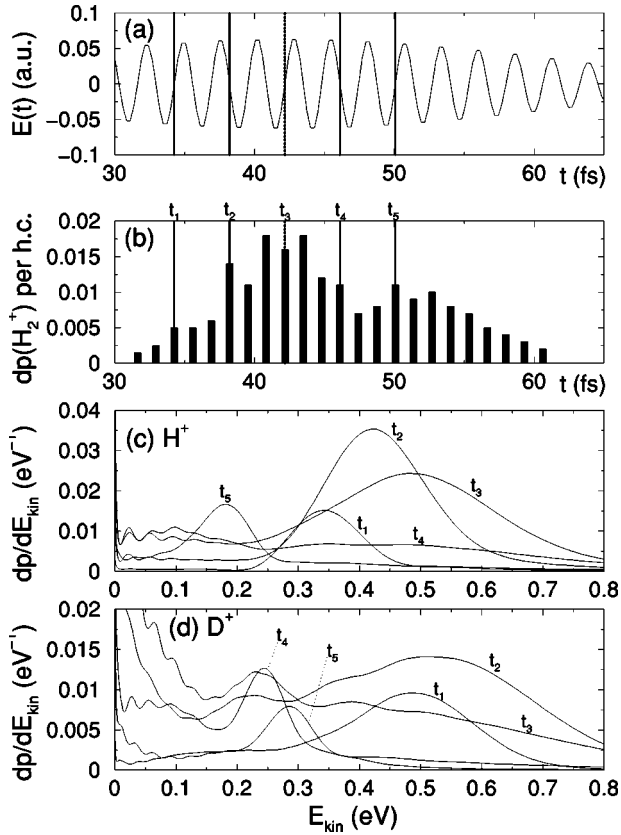


FIG. 5. Same as Fig. 3, but for a 30 fs pulse.

time t_1 was orthogonal to state $|\phi_{t_2}\rangle$ for any $t_1 \neq t_2$. We regard $|\phi_{t_n}\rangle$ as the electronic wave packet produced by one half cycle immediately before t_n , and we add up contributions of different half cycles. So we expect that the condition for incoherent summation is well fulfilled, since the stepwise increase in the ionization probability indicates that the wave packets that are produced by different half cycles are well separated from each other in space, and therefore are almost orthogonal.

For each pulse width, we have sampled 15 equally spaced ionization times around mid-pulse, with spacings of two optical cycles for $\tau_p=80$ fs, one optical cycle for $\tau_p=50$ fs, and one-half optical cycle for $\tau_p=30$ fs. Summation leads to the total spectra plotted in Fig. 6. For $\tau_p=80$ fs, the H^+ peak and the D^+ peak are located at the same kinetic energy. This is consistent with the experimental results. Two competing phenomena are effective here: On one hand, D^+ ions receive larger energy than H^+ ions for equal ionization times; on the other hand, contributions from early ionization times are more important for the dissociation of D_2^+ than in the case of H_2^+ [see panels (c) and (d) of Fig. 3]. For the shorter 50 fs pulse, the maximum of the H^+ peak remains at the same energy, while the D^+ ions receive a larger energy. Note the small maximum on the low-energy side, which we identify with the experimentally observed shoulder mentioned above. If we shorten the pulse width to 30 fs, then the H^+ peak also shifts toward higher energies. Interestingly, the low-energy D^+ ions become so dominant that the peak maximum is now located at a lower energy than the H^+

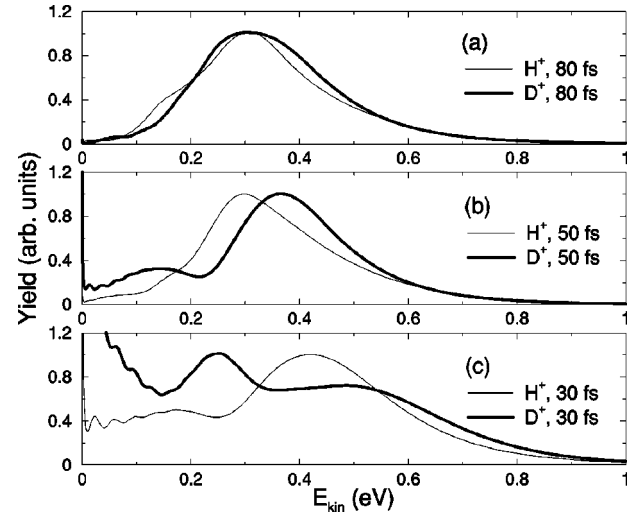


FIG. 6. Calculated kinetic-energy spectra of H^+ and D^+ ions for laser pulses with a peak intensity of 1.5×10^{14} W/cm² and different pulse widths. The spectra are normalized such that the peaks beyond 0.2 eV have a maximum value of 1.

peak. Note, however, that D^+ ions with larger energy are also present in the spectrum.

In the 30 fs and 50 fs spectra we observe unphysical wiggles at low energies. They originate from the fact that bound states near the dissociation threshold are hard to separate from low-energy continuum states and give small additional low-energy contributions to the calculated spectra. Yet we have confirmed the finite probability for zero-energy fragmentation by calculations of energy spectra via the auto-correlation function [27]. This method yields almost identical results for $E_{\text{kin}} > 0.1$ eV, but it does not give low-energy wiggles. It is more time consuming because it requires wavefunction propagation beyond the end of the laser pulse and thus has not been used for the whole bulk of the calculations.

The fact that the calculated peaks are all located at lower energies than in the experiment is due to the one-dimensional model, which has slightly different values for the binding energy and the equilibrium distance.

We may characterize the situation in the following way: If we perform our calculations with 80 fs and 50 fs, then we can well reproduce the trends found in the experiments for 80 fs and 28 fs (isotopic shift and appearance of a low-energy shoulder). In the calculation with 30 fs, these effects become so strong that the kinetic-energy spectra differ qualitatively from the experimental ones. An explanation for this behavior will be given in the next section.

Recently, a pulse-width dependence of the one-photon line was experimentally observed by Frasinski *et al.* [13] which is similar to the behavior of the two-photon line described in the present work. There, the kinetic energy also becomes larger with decreasing pulse duration so that the one-photon peak eventually merges with the two-photon peak, giving rise to a shoulder structure. This is compatible with our calculations since we found for 30 fs pulses that parts of the low-energy fragments stem from one-photon dissociation (see the discussion of Fig. 5). On the other hand, the small D^+ low-energy peak in Fig. 6(b) originates exclu-

sively from two-photon absorption. We therefore believe that the shoulder observed in experiment is a combination of both processes.

VI. INTERPRETATION

In the preceding section, we showed that the experimental findings are reproduced if we add up the kinetic-energy spectra obtained for various times of ionization. Two questions are still open: First, why do D^+ ions tend to receive larger energies, and, secondly, why does the energy release depend on the time of ionization? Simple answers can be given within the adiabatic-dressed-state picture. The nuclei experience an adiabatic potential curve that depends on the laser intensity, and in a short pulse the intensity itself is time dependent. Consequently, the nuclei move in a *time-dependent* potential.

For a laser field with constant intensity, the adiabatic potential surfaces are obtained from Floquet theory [12] or from diagonalization of the R -dependent field-quantized electron-plus-field Hamiltonian [28]. A detailed comparison of the two methods is given in [29,30].

We consider now an extremely simplified model for the dissociation process. At each time step, we diagonalize the 1D electron-plus-field Hamiltonian of H_2^+ (D_2^+), including 40 photon states and only the two lowest electronic states, the gerade ground state $|g(R)\rangle$ and the ungerade first excited state $|u(R)\rangle$ (cf. [30]). Thereby, the possibility of ionization is excluded. A sufficient number of photon states is needed, because the asymptotically divergent transition dipole moment $[\langle u(R)|e_z|g(R)\rangle \approx eR/2$ for large R] leads to asymptotically divergent dressed-state potential curves. If the two electronic states are dressed with a large number of photons (in our case ± 20), then the energy eigenvalues at the lower and upper end of the spectrum still diverge, but the eigenvalues found in the central part of the spectrum form nondivergent and physically correct potential curves. On the other hand, it does not make sense to include even more photon states since higher excited electronic states (which are ignored in this calculation) already lie within the energy range covered by the number of photon states employed here. In order to arrive at a simple picture, we treat the nuclear motion classically using the initial conditions $(R, p_R) = (R_0, 0)$, where R_0 is the equilibrium distance of H_2 (D_2). The nuclei are assumed to follow the adiabatic path that describes a three-photon absorption and subsequent one-photon emission, giving rise to an effective two-photon absorption. (Higher-order curve crossings also exist, but lead to a negligible distortion of the potentials. Diabatic motion is assumed at these points.)

Figure 7 shows the result for a pulse width of $\tau_p = 80$ fs. The time-dependent adiabatic potential is plotted as a surface, starting at the time t_2 of Fig. 3 (two optical cycles before mid-pulse) and ending after the dissociation process is essentially finished. The potential-energy scale is chosen such that for large R the ground state energy of the 1D H (D) atom, -18.2 eV, is recovered. Around mid-pulse, the potential exhibits two minima. The outer minimum at $R \sim 6$ a.u. gradually becomes flatter with increasing time and eventually disappears. (It reappears near the end of the pulse,

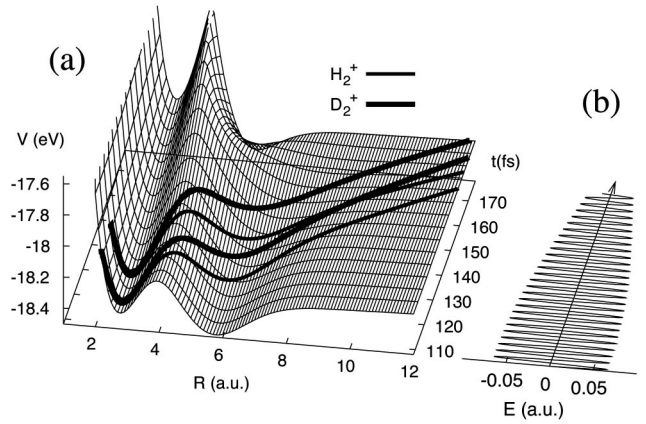


FIG. 7. (a) Time-dependent adiabatic potential for an 80 fs pulse with a peak intensity of 1.5×10^{14} W/cm². Classical trajectories for H_2^+ and D_2^+ are plotted on top of the potential for two different starting times (t_2 and t_4 of Fig. 3). (b) Time-dependent laser field.

but without influencing the dissociation, which is already over then.) For two different times of ionization (t_2 and t_4 of Fig. 3), the classically calculated nuclear coordinate $R(t)$ of H_2^+ and D_2^+ is plotted onto the surface. Along these paths, the nuclei experience a sequence of acceleration and deceleration processes.

First, compare the dynamics of the two isotopes. Since the dissociation of D_2^+ is slower, it needs a longer time to pass the outer minimum in the potential. Consequently, the slow-down on the slope between $R = 6$ a.u. and $R = 9$ a.u. is less effective, leading to a *larger* kinetic energy for D_2^+ . Now, consider the case of two different ionization times. Clearly, the potential experienced by the ion will be different in either case. As one can see from the figure, the accelerating slope between $R = 4$ a.u. and $R = 6$ a.u. is similarly steep in both cases, but the decelerating region $R = 6-9$ a.u. is flatter at later times. As a result, later times of ionization produce faster fragments. Indeed, a close look at the figure reveals that two trajectories belonging to the same isotope but different ionization times have different asymptotic velocities.

The two-state model is very helpful in clarifying the isotopic shift and the importance of the pulse duration. Yet it does not predict the two-photon dissociation probability because it does not allow for ionization of the molecular ion and because we have treated the nuclear motion classically. We saw in the preceding section that this probability depends on the time when H_2 (D_2) is ionized (see Figs. 3–5) and that this is crucial for a full understanding of how the kinetic-energy spectra are formed. In particular, the absence of the isotopic shift in the case of 80 fs pulses can be explained only if these effects are taken into account.

We are now able to explain why there is good agreement of the 28 fs experiment with the 50 fs calculation but less agreement with the 30 fs calculation. By comparison of Table I and Fig. 6 we notice that the fragments are generally slower in the 1D model than in the experiment. Therefore, the complete dissociation process necessarily takes a longer time in the 1D model. We have learned from the

considerations above that the fragments receive a shift toward larger kinetic energies if the dissociation is slow. Thus, the effect should be stronger in the 1D model and should already appear for short pulses of intermediate width, like 50 fs pulses.

In principle, we should take into account the center-of-mass momentum of the molecular ions, which has been estimated to range from -0.6 a.u. to $+0.6$ a.u. (see Sec. III). This would increase the width of the calculated peaks (Fig. 6), which are already broader than the experimental ones. We expect that the calculated peak width will decrease if we employ pulses longer than 80 fs since the contributions from different ionization times (Fig. 3) will cover a smaller energy range if the laser-intensity change during dissociation is slower. Again, this means that we obtain better agreement with experiment if we employ longer pulse durations.

The explanation given by Frasiniski *et al.* [13] for the pulse-width dependence of the one-photon line involved trapping in light-induced bound states. In the effective two-photon dissociation process, the kinetic energy of the dissociating system is sufficiently large to disable trapping in the outer potential well. However, Frasiniski *et al.*'s interpretation and ours agree on the importance of intensity-dependent potential curves. In both cases, the intensity change during the action of a pulse (which apparently depends on the pulse duration) influences the fragment kinetic energies.

VII. CONCLUSION

Our experiments have clearly demonstrated that the ion kinetic-energy spectra obtained from multiphoton fragmentation of H_2 and D_2 depend on the temporal pulse width and on the isotope. These findings have been reproduced in one-dimensional model calculations and interpreted in terms of time-dependent adiabatic dressed states. The fragmentation of H_2^+ is not very sensitive to the pulse width, whereas for D_2^+ the effective two-photon peak shifts toward higher kinetic energies and exhibits a low-energy shoulder for shorter pulses. The effects result from the fact that the pulse width (the time scale for the temporal change of intensity) is comparable to the duration of the dissociation process. Since H_2^+ and D_2^+ dissociate relatively fast, the effect is not very strong, and its detection requires not only short pulses but also a high-resolution setup. We expect that H_2 also exhibits the energy shift if the pulse width is further shortened. Possibly, similar phenomena can be found in heavier molecules as well, where they would be easier to observe due to the slower dissociation.

ACKNOWLEDGMENT

Financial support from the Deutsche Forschungsgemeinschaft is gratefully acknowledged (Schwerpunktprogramm "Time-dependent phenomena and methods in quantum systems of physics and chemistry," Project No. EN 241/6-2).

-
- [1] A. Zavriyev, P.H. Bucksbaum, H.G. Muller, and D.W. Schumacher, *Phys. Rev. A* **42**, 5500 (1990).
 - [2] B. Yang, M. Saeed, L.F. DiMauro, A. Zavriyev, and P.H. Bucksbaum, *Phys. Rev. A* **44**, R1458 (1991).
 - [3] G.N. Gibson, M. Li, C. Guo, and J. Neira, *Phys. Rev. Lett.* **79**, 2022 (1997).
 - [4] T.D.G. Walsh, F.A. Ilkov, and S.L. Chin, *J. Phys. B* **30**, 2167 (1997).
 - [5] M.R. Thompson, M.K. Thomas, P.F. Taday, J.H. Posthumus, A.J. Langley, L.J. Frasiniski, and K. Codling, *J. Phys. B* **30**, 5755 (1997).
 - [6] T.D.G. Walsh, F.A. Ilkov, S.L. Chin, F. Châteauneuf, T.T. Nguyen-Dang, S. Chelkowski, A.D. Bandrauk, and O. Atabek, *Phys. Rev. A* **58**, 3922 (1998).
 - [7] M.E. Sukharev and V.P. Krainov, *Zh. Éksp. Teor. Fiz.* **110**, 832 (1996) [*JETP* **83**, 457 (1996)].
 - [8] H. Rottke, C. Trump, and W. Sandner, *Laser Phys.* **9**, 171 (1999).
 - [9] C. Trump, H. Rottke, and W. Sandner, *Phys. Rev. A* **59**, 2858 (1999).
 - [10] A. Giusti-Suzor, F.H. Mies, L.F. DiMauro, E. Charron, and B. Yang, *J. Phys. B* **28**, 309 (1995).
 - [11] J. Ludwig, H. Rottke, and W. Sandner, *Phys. Rev. A* **56**, 2168 (1997).
 - [12] J.H. Shirley, *Phys. Rev.* **138**, B979 (1965).
 - [13] L.J. Frasiniski, J.H. Posthumus, J. Plumridge, K. Codling, P.F. Taday, and A.J. Langley, *Phys. Rev. Lett.* **83**, 3625 (1999).
 - [14] J.H. Posthumus, L.J. Frasiniski, A.J. Giles, and K. Codling, *J. Phys. B* **28**, L349 (1995).
 - [15] T. Zuo and A.D. Bandrauk, *Phys. Rev. A* **52**, R2511 (1995).
 - [16] T. Seideman, M.Y. Ivanov, and P.B. Corkum, *Phys. Rev. Lett.* **75**, 2819 (1995).
 - [17] S. Chelkowski, C. Foisy, and A.D. Bandrauk, *Phys. Rev. A* **57**, 1176 (1998).
 - [18] J.H. Posthumus, J. Plumridge, P.F. Taday, J.H. Sanderson, A.J. Langley, K. Codling, and W.A. Bryan, *J. Phys. B* **32**, L93 (1999).
 - [19] R. Moshhammer, B. Feuerstein, W. Schmitt, A. Dorn, C.D. Schroter, J. Ullrich, H. Rottke, C. Trump, M. Wittmann, G. Korn, K. Hoffmann, and W. Sandner, *Phys. Rev. Lett.* **84**, 447 (2000).
 - [20] J.H. Posthumus, J. Plumridge, K. Codling, L.J. Frasiniski, A.J. Langley, and P.F. Taday, *Laser Phys.* **9**, 163 (1999).
 - [21] J.H. Eberly, Q. Su, and J. Javanainen, *Phys. Rev. Lett.* **62**, 881 (1989).
 - [22] D.G. Lappas and R. van Leeuwen, *J. Phys. B* **31**, L249 (1998).
 - [23] H. Yu, T. Zuo, and A.D. Bandrauk, *Phys. Rev. A* **54**, 3290 (1996).
 - [24] K.C. Kulander, F.H. Mies, and K.J. Schafer, *Phys. Rev. A* **53**, 2562 (1995).
 - [25] J.C. Wells, I. Simbotin, and M. Gavrilu, *Phys. Rev. A* **56**, 3961 (1997).
 - [26] T. Cheng, J. Liu, and S. Chen, *Phys. Rev. A* **59**, 1451 (1999).
 - [27] M.D. Feit, J.A. Fleck, Jr., and A. Steiger, *J. Comput. Phys.* **47**, 412 (1982).
 - [28] See, e.g., C. Cohen-Tannoudji, J. Dupont-Roc, and G. Grynberg, *Atom-Photon Interactions: Basic Processes and Applications* (Wiley, New York, 1992), Chap. VI.
 - [29] F.H. Mies and A. Giusti-Suzor, *Phys. Rev. A* **44**, 7547 (1991).
 - [30] R.W. Heather and F.H. Mies, *Phys. Rev. A* **44**, 7560 (1991).